GFRP-Reinforced Concrete Slabs: Fire Resistance and Design Efficiency

Hamzeh Hajiloo[1]; Mark F. Green[2]; Martin Noël[3]; Noureddine Bénichou[4]; and Mohamed Sultan[5]

Abstract: Thickening concrete cover to obtain an adequate fire resistance lowers the efficiency of glass fiber–reinforced polymer (GFRP) reinforcement and increases the cost relative to conventional steel reinforcement. This paper investigates the fire resistance of two full-scale GFRP-RC slabs with only 40 mm of clear concrete cover and 200 mm of unexposed (cool) anchor zone at the ends. Both slabs endured 3 h under the standard fire. The slabs were loaded with a sustained load, which caused a moment equal to 45% of their ultimate flexural strength. Emphasis was placed on studying the bond behavior of GFRP bars by comprehensively investigating temperature distributions particularly at the unexposed anchor zones at the ends of the slabs. The temperature reduces significantly in the unexposed zones, providing an adequate anchorage for the bars when almost the entire GFRP-to-concrete bond deteriorated in the exposed zone. The analysis of the experimental results showed that the increase in the tensile force in the GFRP bars during the standard fire is below 50% of the existing sustained force. A new model considers the bond degradation to predict the fire resistance of GFRP-reinforced slabs. The results enable an efficient, economic, and fire-safe application of GFRP reinforcement in concrete construction by reducing the concrete cover. **DOI: 10.1061/(ASCE)CC.1943-5614.0000937.**

Author keywords: Glass fiber–reinforced polymer (GFRP)–reinforced concrete; High temperatures; Bond deterioration; Fire resistance.

Introduction

Concrete elements reinforced with glass fiber–reinforced polymer (GFRP) are commonly assumed to have lower fire resistance than equivalent conventional steel-reinforced concrete ones. Until the latest version of ACI 440.1R (ACI 2015), the application of fiber-reinforced polymer (FRP) reinforcing bars was not recommended where fire resistance was vital to maintain structural integrity. The enhanced confidence in fire performance of GFRP bars was attained as a result of experimental studies (Bisby and Kodur 2007; Nigro et al. 2011a; Hajiloo et al. 2018). A conservative approach was adopted by CSA S806 (CSA 2012), which proposes thick concrete cover (i.e., 60 mm for 2 h of fire resistance) to delay the deterioration of GFRP bars during the fire. However, such thicker concrete cover results in inefficient material use in GFRP-reinforced concrete. Because the GFRP costs relatively more than conventional black steel, efficient use of the material is essential. Therefore, this paper investigates the performance of GFRP-RC slabs in fire with only 40 mm of clear concrete cover to develop more efficient approaches for achieving fire resistance.

[1]Postdoctoral Fellow, Dept. of Civil Engineering, Queen's Univ., Kingston, ON, Canada K7L 3N6 (corresponding author). Email: Hajiloo.h@queensu.ca

[2]Professor, Dept. of Civil Engineering, Queen's Univ., Kingston, ON, Canada K7L 3N6.

[3]Assistant Professor, Dept. of Civil Engineering, Univ. of Ottawa, Ottawa, ON, Canada CBY A513.

[4]Senior Research Officer, NRC-Construction, National Research Council Canada, Ottawa, Canada K1A 0R6.

[5]Senior Research Officer, NRC-Construction, National Research Council Canada, Ottawa, Canada K1A 0R6.

Note. This manuscript was submitted on November 21, 2017; approved on October 16, 2018; published online on February 15, 2019. Discussion period open until July 15, 2019; separate discussions must be submitted for individual papers. This paper is part of the ***Journal of Composites for Construction***, © ASCE, ISSN 1090-0268.

Literature Review

The concerns regarding GFRP-reinforced concrete in fire were articulated when several full-scale fire tests revealed serious damage to the bars and premature failure of GFRP-RC elements. Abbasi and Hogg (2006) tested two GFRP-RC beams with different types of reinforcing bars. Beam-1 was reinforced using bars with thermoset resin, while Beam-2 was reinforced with bars with thermoplastic resin. The total reinforcement ratio was the same for both beams. Although the exact information was not provided to determine the unexposed length of the bars at the ends, the beams both failed due to rupture of the bars at midspan. This shows that an adequate bond was provided at the ends that allowed the tensile rupture of the GFRP bars. Inferior fire performance was observed for Beam-2, which was reinforced with bars manufactured with thermoplastic resin. Nonetheless, the superior performance of Beam-1 with thermoset resin cannot certify that thermoset resin necessarily acts better than thermoplastic resin at elevated temperatures because the earlier study by Kumahara et al. (1993) showed that bars with thermoplastic resin [namely, polyphenylene sulfide (PPS)] may have higher heat resistance than vinyl ester resin, which is thermoset. In the beams tested by Abbasi and Hogg (2006), the resin content of the bars was not provided in the literature, although it was shown that bars with thermoplastic resin lost more weight due to fire exposure, which implies higher resin content of the bars. The lower fire resistance of Beam-2 can be attributed to the higher resin content that makes the reinforcing bars more vulnerable at elevated temperatures. In addition, the fire test of Beam-1 and Beam-2 was conducted 38 days after casting the beams, which means higher water content was present in the beams during the fire test, causing noticeable spalling of the beams. Although the concrete cover was thick (70 mm) and the beams were loaded only with 40 kN (2/3 of the cracking load and 13% of the failure load at room temperature), Beam-1 and Beam-2 endured 128 and 94 min, respectively. Based on the outcome of the fire test, Abbasi and Hogg recommended 70-mm clear concrete cover to achieve 90 min of fire resistance

for GFRP-RC beams. The fire test by Weber (2008) showed that the reinforcement layout in GFRP-RC slabs cannot be arbitrary if fire safety is required. The slab in Weber's experiment failed due to the complete loss of bond strength of the spliced GFRP bars at mid-span. With 60-mm clear concrete cover, the reinforcing bars reached 225°C after 90 min with a gradual degradation in bond strength, which resulted in collapse.

Although the previously mentioned experimental studies raised concerns regarding fire safety and an efficient application of GFRP bars in concrete, experimental studies (Nigro et al. 2011a; Hajiloo et al. 2017) showed that the bond failure of fire-exposed GFRP-RC slabs can be prevented by providing sufficiently long unexposed (cool) regions to ensure adequate anchorage of the bars. As a part of a research study on the behavior of GFRP reinforcing bars at elevated temperatures, two full-scale slabs were tested in the floor furnace at the National Research Council (NRC) Canada facilities. The slabs were designed and fabricated based on the findings from the previous fire tests on GFRP-RC slabs by Hajiloo et al. (2017). The objectives of the study presented in the current paper are to

1. determine the fire performance of GFRP-reinforced slabs with only 40 mm of clear concrete cover and with only 200 mm of unexposed (cool) anchor zones at the ends in contrast to previous work with more cover (60 mm);
2. experimentally examine the temperature distribution along the unexposed anchorage length with substantial instrumentation in the unexposed anchor zones;
3. study the tensile force condition in the GFRP bars during fire and provide an estimation of the tensile force by evaluating the experimental data; and
4. develop a new model to predict the fire resistance of GFRP-RC slabs based on the retained bond strength and the numerical heat transfer analysis that was presented in Hajiloo et al. (2017).

This paper presents new, original, and important information on the fire performance of GFRP-RC slabs that the efficient design and use of GFRP bars is not compromised to obtain an adequate fire resistance. The GFRP-reinforcement ratio of the slabs with 40 mm of cover was reduced to 2/3 of the slabs with 60-mm cover. Additionally, a novel and fundamental understanding of temperature distributions was obtained through a systematic instrumentation in the unexposed anchor zones.

Experimental Program

The intended purpose of the current fire test was to achieve 2 h of fire resistance with only 40-mm cover for simply supported unrestrained slabs under standard fire; CSA S806 (CSA 2012) requires 60-mm cover to achieve the same resistance. Two concrete slabs were fabricated that were identical in every aspect except the type of GFRP reinforcing bars. The slabs were 3,900 mm long, 1,200 mm wide, and 200 mm thick, which is typical for slabs in many applications such as parking garages. The clear concrete cover to the bottom of the longitudinal reinforcing bars was 40 mm. The center-to-center spacings of the bottom and top longitudinal reinforcement were 150 and 220 mm, respectively. The balanced reinforcement ratio was 0.15%, and the reinforcement ratio of the bottom reinforcing bars was 0.88%. The transverse reinforcing bars were placed at 200-mm intervals in the bottom and top meshes to control shrinkage and thermal cracks.

Materials

The two slabs were labeled as Slab-A and Slab-B. Slab-A was reinforced with GA bars and Slab-B with GB bars. The GA bars utilized sand coating on the surface, which was applied on the hardened reinforcing bar following the pultrusion process. The GB bars had a helical braid of fibers in addition to a sand coating (Fig. 1). The GA (Pultrall, Thetford Mines, Quebec, Canada) and GB (TUF-BAR, Alberta, Canada) reinforcing bars with a nominal diameter of 16 mm (#5 bars) were received from two different manufacturers, and the reported properties by the manufacturers are summarized in Table 1. The ultimate tensile capacities were 340 and 256 kN for GA and GB, respectively. The actual average cross-sectional areas of GA and GB bars were measured by the immersion method as instructed by CSA S806 (CSA 2012). The actual average cross-sectional areas and the equivalent diameters of the bars were higher than the nominal values. The nominal values were used to define the nominal tensile strength and modulus of elasticity, and these values were used throughout this paper. The glass transition temperature (T_g) was determined by the differential scanning calorimetry (DSC) method according to CSA S807 (CSA 2010).

Carbonate aggregate with a maximum size of 20 mm was used in the concrete. The compressive strength of the concrete was measured by crushing standard concrete cylinders (100 × 200 mm) according to CSA A23.1-14/A23.2-14 (CSA 2015). The average compressive strength at 28 days was 34.0 MPa with the standard deviation of 0.9 MPa. The compressive strength of the concrete was also measured before the fire test (6 months after concrete cast), which was 36.6 MPa with a standard deviation of 1.2 MPa.

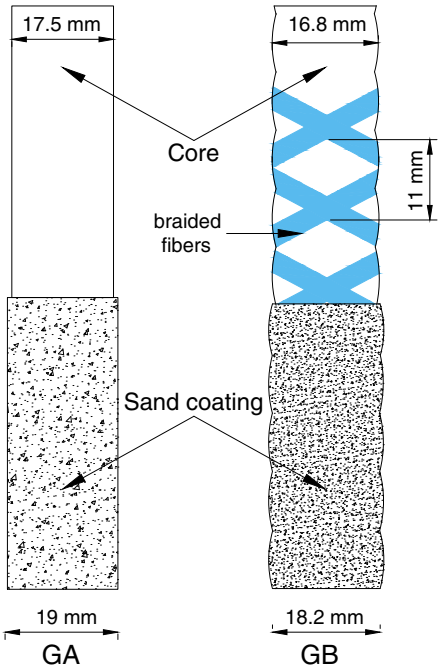

Fig. 1. GFRP reinforcing bars.

Table 1. Material properties of the bars

Property	GA (#5)	GB (#5)
Actual cross-sectional area (mm^2)	280	252
Equivalent diameter (mm)	19	18
Nominal diameter (mm)	16	15
Nominal cross-sectional area (mm^2)	200	200
Nominal tensile strength (MPa)	1,700	1,280
Nominal modulus of elasticity (GPa)	64.1	62.6
Ultimate elongation (%)	2.7	2.1
Fiber content (% by weight)	80.7	82.9
Glass transition temperature (°C)	110	114

Test Setup

The floor furnace is equipped with a movable steel rig to mount the slabs on top of the furnace. The slabs were placed side by side with ceramic insulating blankets between them on the floor furnace. Figs. 2(a and b) show the setup of the slabs on the furnace from above and underneath. The furnace is equipped with protected thermocouples, which were placed close to the bottom of the slabs, to maintain the temperature near the bottom surface of the slabs at the desired temperature. The standard fire test was performed according to the provisions of ASTM E119 (ASTM 2015). Closely following the ASTM E119 fire curve, the temperature increased rapidly during early stages and stabilized at around 1,000°C and slowly reached 1,050°C in 3 h. The uniformly distributed load was applied by a loading system that included six jacks for each slab as shown in Fig. 2(c). The superimposed load was constant during the fire test until failure occurred.

Fig. 3 illustrates a cross section of the furnace with one slab placed on the frame. The slabs were tested without end restraints and were free to rotate and expand. The slabs were deliberately allowed to expand and move at both sides so that the unexposed zones at the ends would remain equal at both sides. A sufficient gap length (30 mm) was provided at the ends so that the slab could freely expand upon loading and heating. Heat-insulating layers were 50 mm thick and placed on the bottom surfaces of the slabs at the ends. Refractory ceramic fiber (RCF) materials that can function up to 1,400°C were used to protect the steel rig and the ends of the slabs. With the low thermal conductivity, the 50 mm of RCF layers keeps the temperature on the cold face at 100°C when the hot face is 1,100°C. Considering the support length, approximately 200 mm of the ends of each slab were protected from direct fire exposure, which is referred to as unexposed zones in the paper hereafter. The main reinforcing bars were 3,890 mm long with only 5-mm concrete cover on the extremities. The test setup and fire exposure condition are shown in Fig. 3.

Instrumentation

The slabs were instrumented to collect an extensive set of data to investigate temperature distributions in both fire-exposed and unexposed zones. Primary emphasis was placed on acquiring the temperature data in unexposed zones because earlier experiments by the authors revealed that the failure behavior is governed by the bond performance of reinforcing bars at the ends. Moreover, the temperature readings in the exposed zones showed that heat was uniformly distributed in the furnace and penetrated within the slab thickness (Hajiloo et al. 2017). Fig. 4 shows the layout of the bottom reinforcing bars and Section C-C, which contains most of the thermocouples. The schematic layout and positions of other instruments are also shown in this paper where the respective results are presented. In total, 23 thermocouples were installed in unexposed zones of each slab. The demonstrated thermocouples in the unexposed zones (Fig. 4) were installed at a depth of 40 mm. To prevent disturbing the GFRP-to-concrete bond over the main

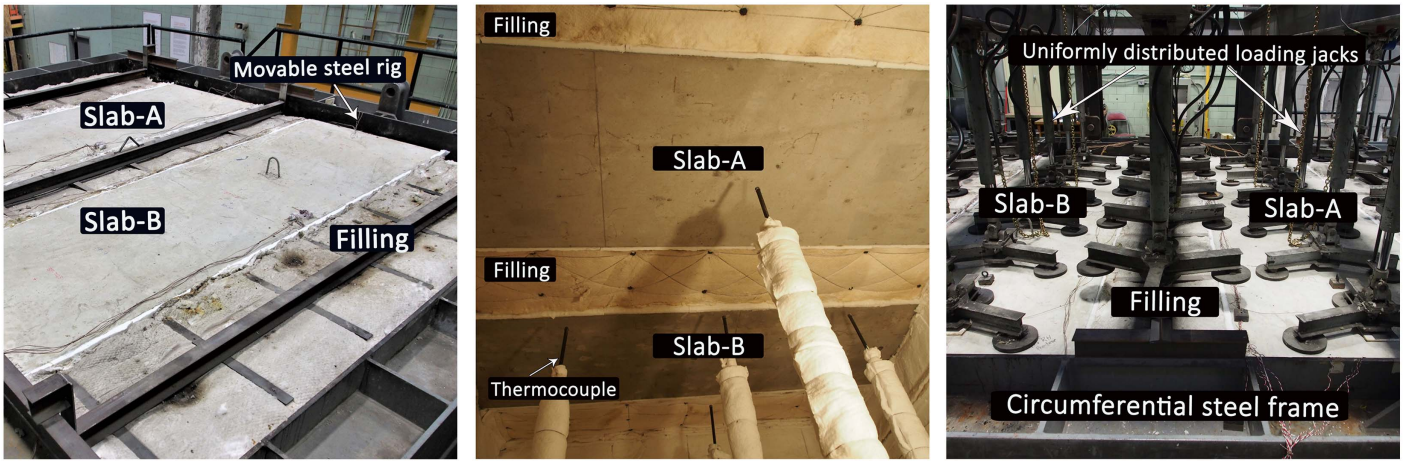

Fig. 2. Floor furnace: (a) preparation after placing the slabs on top; (b) view from inside and the protected thermocouples; and (c) loading pads aligned on the slabs.

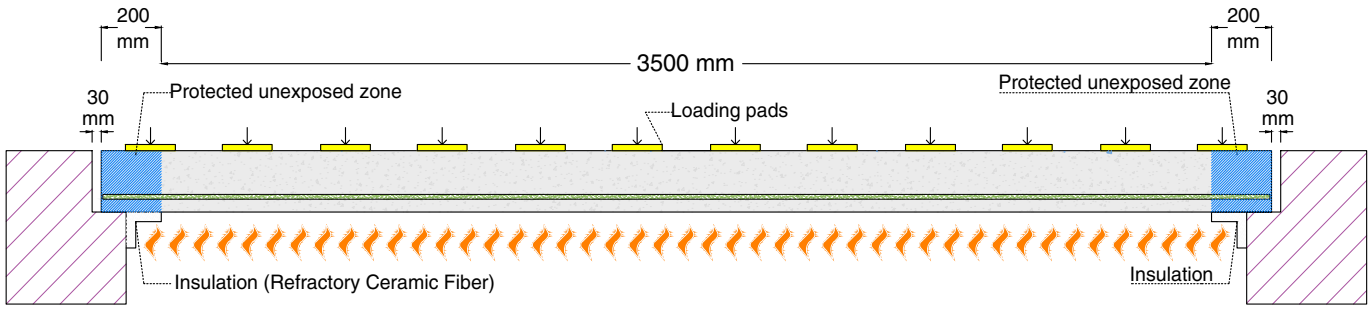

Fig. 3. Fire test setup.

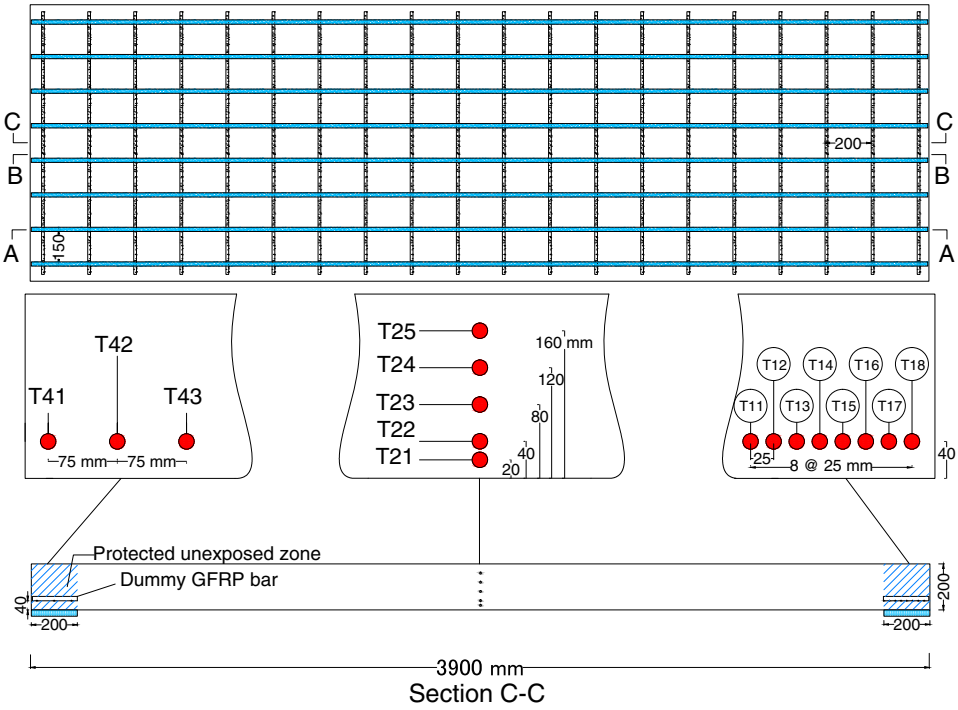

Fig. 4. Instrumentation details.

longitudinal bars, two short (200-mm) dummy bars were used to install thermocouples. The first thermocouple was placed 25 mm from the end of the slabs and the remaining thermocouples were installed at 25-mm intervals; the last thermocouple was located at the boundary of the exposed and unexposed zones. There were 12 thermocouples in Sections A-A and B-B to investigate the temperature distribution at various positions within the unexposed zones. At midspan, five thermocouples were placed within the thickness of the slabs. In order to monitor heat transfer at the top surface of the slabs, three thermocouples were used to ensure that the average temperature remained below 140°C at the top unexposed surface throughout the fire test as required by ASTM E119 (ASTM 2015).

Regardless of the inherent delicacy of strain gauges at elevated temperatures, strain gauges are still used for measuring strains and stress in concrete and reinforcing bars. Strain gauges were installed on reinforcing bars at midspan to measure strains before the fire test under sustained loads and during the early minutes of the fire test. Electrical resistance strain gauges (5 mm long) with a functional temperature range of −75°C to +95°C were installed on the GFRP bars over an area where the sand coating was removed. Two long strain gauges were installed on the top surface of the slabs to measure the compression strains under sustained loads as well as the thermally induced strains in the concrete. The strain gauges were 60 mm long with the functional temperature of 80°C.

Design of Slabs

Serviceability criteria including deflection and crack width were checked using three common FRP-RC codes and guidelines including ACI 440.1R (ACI 2015), CSA S806 (CSA 2012), and ISIS Canada Design Manual 3 (ISIS Canada 2007).

Table 2 summarizes the predicted results for deflections and crack widths at five moment levels ($M_a = 27$, 40, 45, 52, and 61 kN · m). The main difference among the guidelines that were used to calculate the midspan deflection is the formula for the effective moment of inertia (I_e). In general, ACI 440.1R (ACI 2015) gives lower deflection values than the others in Table 2. The deflection values from ISIS Canada Design Manual 3 (ISIS Canada 2007) and CSA S806 (CSA 2012) are relatively close except for 27 kN · m. This is because ISIS Canada Design Manual 3 adopts a conservative calculation of I_e where it reduces the I_e even if the applied total moment is less than the cracking moment.

Considering the live-load deflection limit as $l_n/360$ from the serviceability criteria in CSA S806 (CSA 2012), and assuming the same deflection under dead-load effects, then the total deflection limit would be 21 mm. Furthermore, CSA S806 (CSA 2012) allows crack widths of 0.5 mm for exterior and 0.7 mm for interior applications. From the serviceability calculations, the service limits for cracking and deflection were exceeded for moments above 40 kN · m. As a compromise between the ultimate load and service load requirements, the test superimposed load was chosen as a

Table 2. Serviceability conditions design for Slab-A

		Moment (kN · m)				
Parameter	Standard	27	40	45	52	61
Total deflection (mm)	ACI 440.1R5	1	18	21	29	42
	ISIS Canada Design Manual 3	12	29	32	39	51
	CSA S806	3	33	36	43	55
Crack width (mm)	ISIS Canada Design Manual 3	0.50	0.78	0.83	0.97	1.20

distributed load of 19.1 kN/m, causing a total moment of 45 kN · m at midspan, which is 45% of the ultimate flexural capacity of the slabs. It was conservatively assumed that the slabs will carry a live load of 6 kN/m^2 and the self-weight dead load. If the dead- and live-load factors are 1.25 and 1.5, respectively, the factored service moment would be 32.5 kN · m. Thus, the slabs were loaded to a notably heavy sustained load, which is approximately 50% higher than the expected factored service loads, before and during the fire test.

Experimental Results

The internal relative humidity (RH) values of the slabs were 75% and 71% for Slab-A and Slab-B. The RH values were measured by drilling a hole 75 mm deep at the corner of each slab and using a humidity probe. The holes were made at the corners so that the integrity of the slabs was not disturbed. Some local and small spalling occurred in the first hour of fire but did not influence the slab's integrity. Visual inspection after the test showed concrete flaking on the bottom surface. In a few locations, the slabs lost some thickness of concrete up to 10 mm. Regardless, the integrity of the remaining concrete was observed to be in an undamaged condition. This was verified when the concrete cover was removed from a few defined locations to uncover the reinforcing bars for assessment purposes. Consequently, the heat propagation in the slabs was normal without abrupt changes due to concrete loss. The experimental results are presented in the following sections.

Temperature Variation

Temperature distribution in various sections of the slabs is a critical factor in defining the overall behavior of fire-exposed elements. The changes in material properties, either concrete or reinforcing bars, take place with the evolution of heat within the element. Thus, the comprehensive data were collected from the critical positions during the fire. The protective and insulating role of concrete is beneficial for reinforcing bars to delay the degradation of mechanical properties at high temperatures. Fig. 5 demonstrates the temperature variations as a function of fire exposure time within the depth of the slabs at midspan. The temperatures at the various depths of 10, 20, 40, 60, and 80 mm were measured. Measurements at 40 and 60 mm represent temperatures at the bottom and top of the reinforcing bars. The recorded temperatures at 10 and 20 mm were quite extreme, reaching around 900°C and 750°C, respectively, after 3 h. The great temperature difference between the readings at 20 and 40 mm shows the significant function of concrete cover in protecting reinforcing bars. Although there is a big difference between temperatures at 20 and 40 mm, temperature variations within the thickness at 40, 60, and 80 mm reached a steady condition. This encourages the placement of reinforcing bars with a clear concrete cover of not less than 40 mm.

A notable spike was recorded particularly at the depths of 10 and 20 mm at around 75 min. Notwithstanding the local and small spalling of concrete, the previously mentioned spikes were due to local temperature variations in the furnace. The temperature in the furnace was programmed to follow the ASTM E119 time-temperature curve. The average of readings from nine thermocouples in the furnace [Fig. 2(b)] was used to control the fuel flow and temperature. A temperature variation of up to 250°C among the controlling thermocouples was recorded at 75 min, causing short-time inconsistent temperatures in various locations of the furnace. As seen in Fig. 5, the time length of the spikes was approximately 25 min.

While the temperature at the bottom of the reinforcing bars increased to 460°C after 3 h, the temperature at the top of the bars was 340°C, indicating a thermal gradient of 120°C across the bars. The temperature distribution data were also collected from the unexposed anchor zones where eight thermocouples were aligned over a length of 200 mm. These areas of interest were heavily instrumented since the failure of the slabs was expected to initiate by GFRP-to-concrete bond degradation based on a previous set of fire tests (Hajiloo et al. 2017). The results (Fig. 6) showed that the temperatures remained below 100°C at 75 mm from the ends of Slab-A during the entire fire exposure; the maximum temperature at the same location for Slab-B was 116°C. At these temperatures, the bond strength between the concrete and the GFRP was approximately 30% of the room-temperature strength (Hajiloo and Green 2018). Temperatures drop significantly from the edge of the exposed zone toward the end, especially between 200 and 125 mm from the end of the slabs. The thermal field becomes more uniform at the end 75 mm.

Several thermocouples were placed at various depths in the unexposed zones to thoroughly investigate the thermal field in the unexposed zones and measure the effectiveness of the heat-insulating layer. Figs. 7(a and b) show that the temperatures at the bottom of the slabs reduce significantly toward the end of

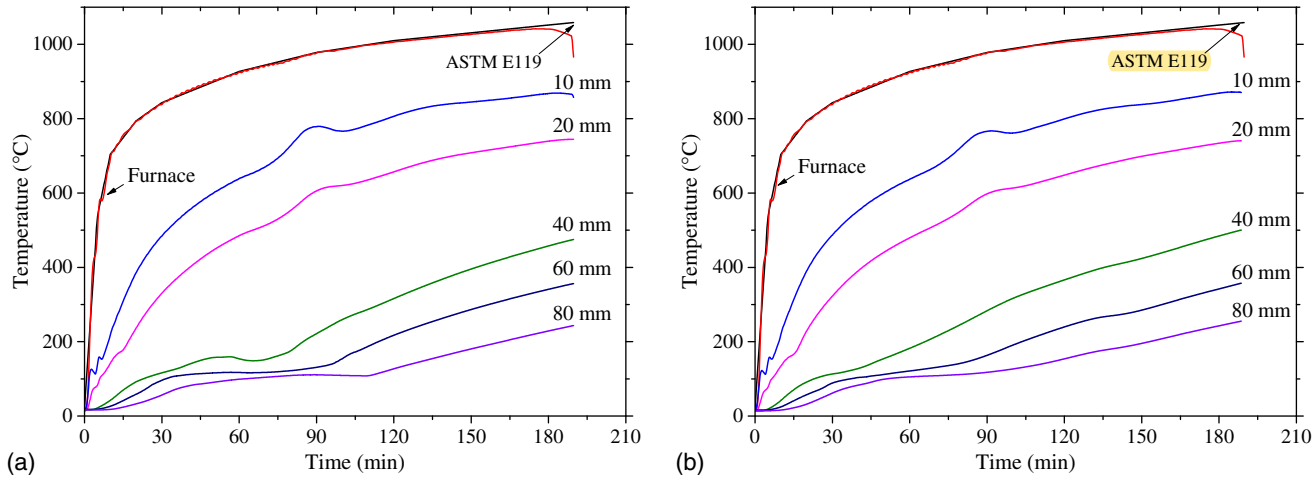

Fig. 5. Temperatures within the thickness of slabs during fire exposure: (a) Slab-A; and (b) Slab-B.

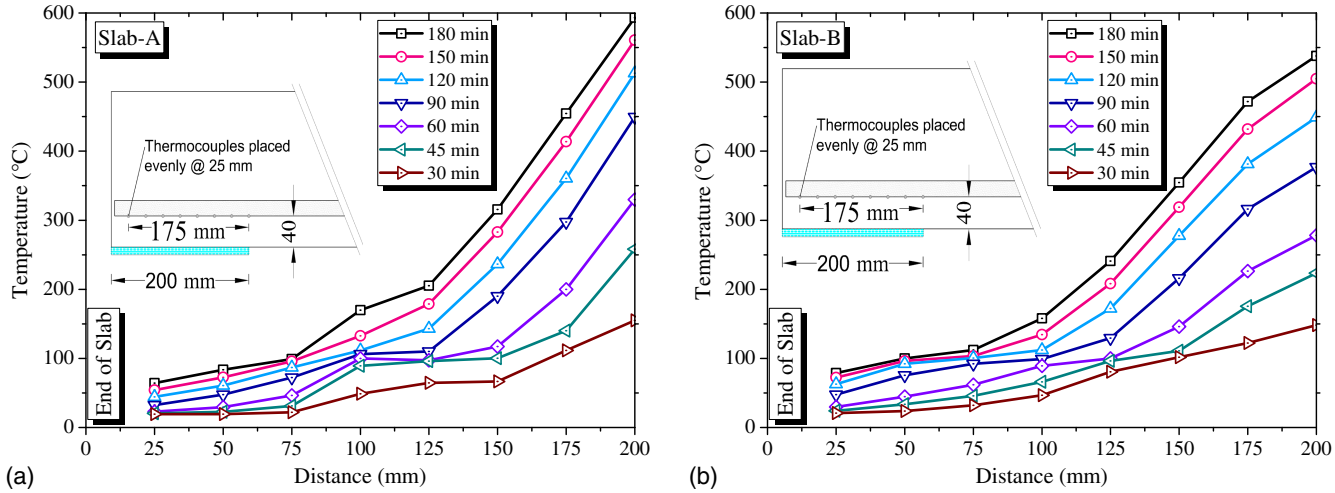

Fig. 6. Temperature gradients in unexposed zones: (a) Slab-A; and (b) Slab-B.

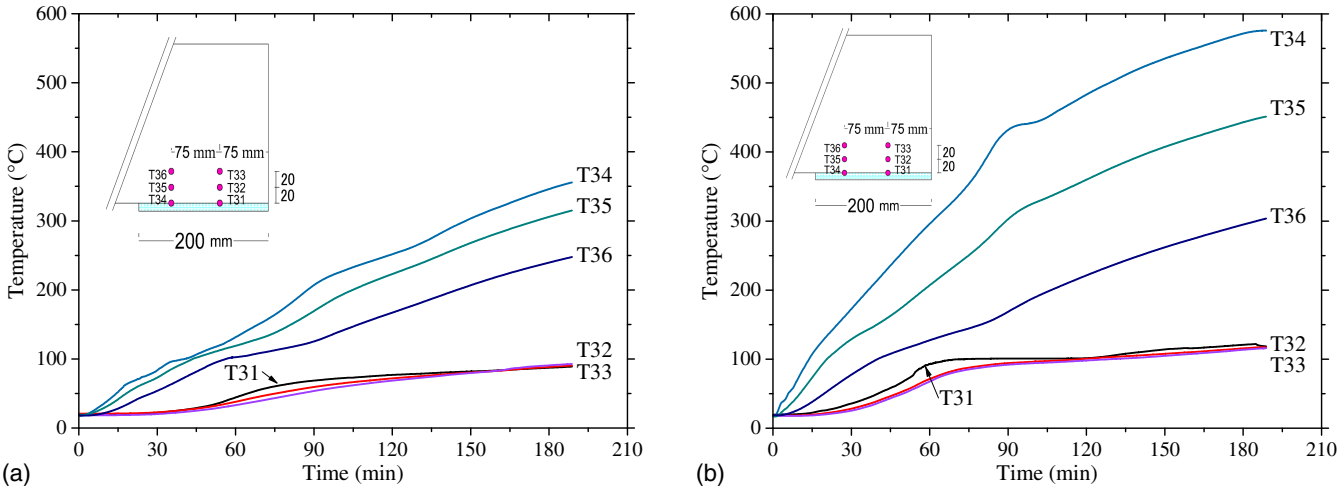

Fig. 7. Temperatures in unexposed zones: (a) Slab-A; and (b) Slab-B.

the slabs. In general, the intensity of heat diminished with increasing distance from the heat-exposed zone. The measurements at 150 mm in Slab-B show higher heat intensity than Slab-A, which can be attributed to some variances in the thermocouple's positions and slight variances in the width or alignment of the heat-insulating ceramic fabric. However, the temperature distribution was consistent at 75 mm from the ends of both slabs.

The temperature measurements presented in Fig. 8 provide a basis to evaluate the conditions of top reinforcing bars in restrained or continuous multispan elements. The temperature distribution at the top part of the concrete cross section is important to determine the temperatures at the negative reinforcement near the supports. The thermocouples were placed at 150 mm from the end of Slab-A and the temperatures were measured at 10, 40, 80, and 120 mm from the bottom of the slabs [Fig. 8(a)]. In addition, the measurements at 75 mm from the end of Slab-A showed a slight temperature increase as temperatures at depths of 100 and 160 mm reached 70°C and 50°C, respectively, after 3 h [Fig. 8(b)].

Load and Deflection Behavior

The specified superimposed load was applied in four steps with 15-min intervals between each step. Fig. 9 shows the superimposed moment–deflection diagrams where a similar behavior can be seen for both slabs. The slabs were indeed subject to a high level of superimposed load to simulate critical situations during a fire incident. The applied load was considerably beyond the expected load on such slabs in a real fire incident.

Fig. 10(a) shows the time–deflection behavior of the slabs during the fire. Nonlinear thermal gradient within the depth of the slabs caused the thermal bowing of the slabs. The deflection consisted of rapidly developed thermal bowing deflection and the gradual deflection due to the degrading properties of concrete and reinforcing bars as temperature rises. Temperature increased at the bottom layers of concrete very quickly, causing a rapid deformation in the first 20 min of fire, and afterward the slabs deformed at a slower rate. After 60 min, the temperatures at the bottom of the reinforcing bars in the exposed zone reached 180°C, at which time the remaining bond strength of the reinforcing bars is small (around 10%) according to the pullout tests that were performed on the same types of the bars at high temperatures (Hajiloo and Green 2018). However, the relatively short embedment of the reinforcing bars into the unexposed anchor zone still provided sufficient bond strength. In other words, the slabs were anchored from both ends, acting like a tied arch.

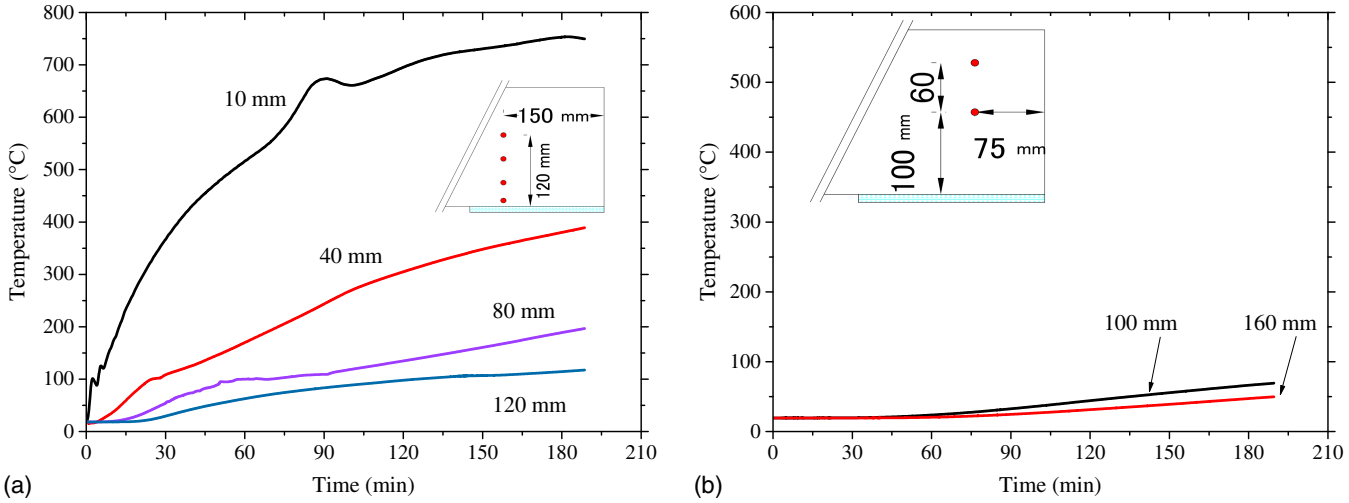

Fig. 8. Temperature variations within the thickness of Slab-A in the unexposed zone at (a) 150 mm from the end; and (b) 75 mm from the end.

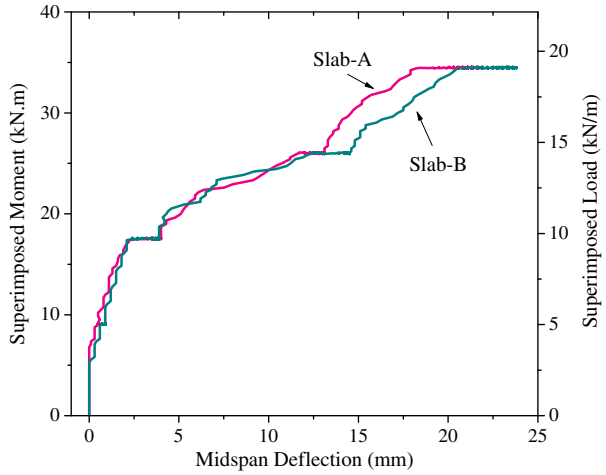

Fig. 9. Loading before fire exposure.

Both slabs, especially Slab-B, showed a higher rate of deformation at 105 min, yet slower than the rate of thermal bowing at the beginning of the fire. Right after 3 h (at 188 min), Slab-B failed with excessive deformations that left a gap between the slabs on the furnace where flames leaped through. The test was stopped to prevent Slab-B from falling into the furnace and causing damage to the furnace. Fig. 10(b) shows the deflection behavior versus temperature in the furnace. The furnace temperature reached 800°C and 1,000°C in 30 and 75 min, respectively.

Failure Modes and Visual Observations

According to ASTM E119 (ASTM 2015), the average temperature rise of the unexposed surface of slabs with respect to the room temperature has to remain below 140°C. In addition, the passage of flame through slabs is not permitted. None of these failure criteria associated with thermal behavior occurred during the fire exposure.

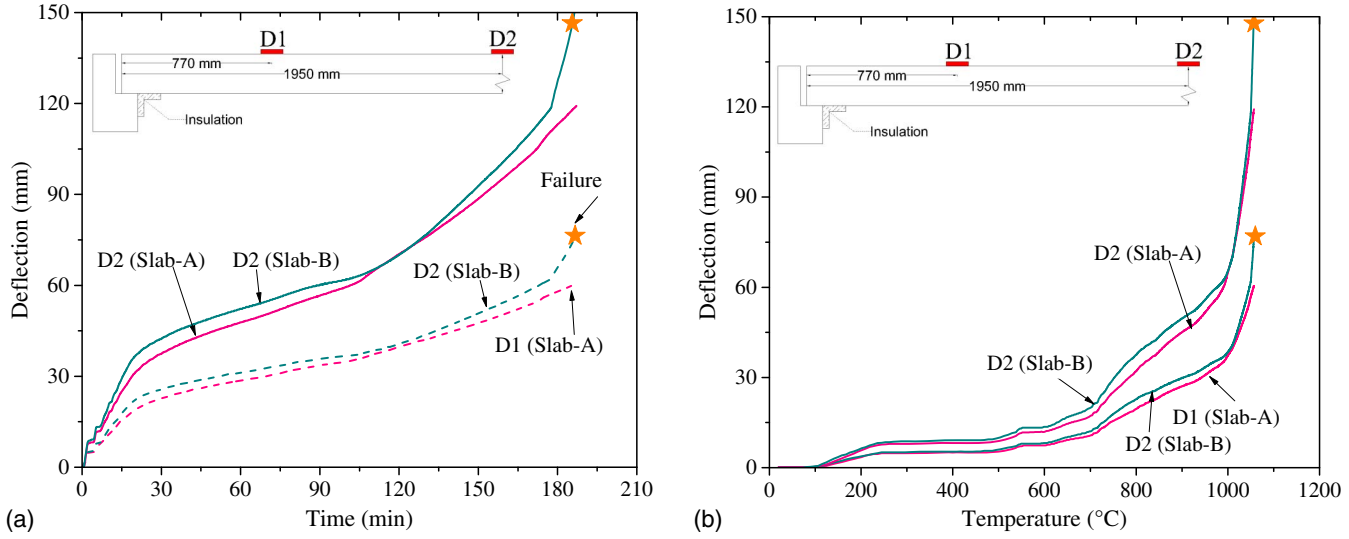

Fig. 10. Deflection of the slabs during the fire as a function of (a) fire exposure time; and (b) furnace temperature.

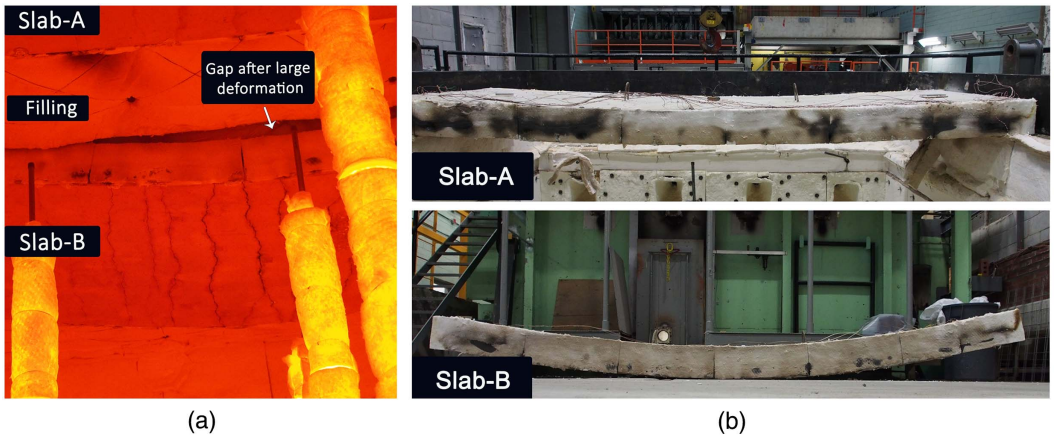

Fig. 11. (a) Failure time of Slab-B seen from the furnace; and (b) Slab-A and Slab-B after the fire test.

Slab-B endured 3 h of standard fire exposure under a sustained moment of 45 kN · m that corresponded to 45% of the ultimate flexural strength of the slabs based on concrete compressive strength at 28 days. Fig. 11(a) shows a view of the inside of the furnace at the time when Slab-B failed. Excessive transverse cracks are visible on the bottom surface of Slab-B. The other slab did not fail and was removed to be tested at room temperature to investigate the postfire residual remaining strength. Slab-A and Slab-B are shown in Fig. 11(b) a day after the fire test. The image of Slab-A was taken when the slab was still on the floor furnace, and the permanent deformation (approximately 25 mm) of the slab can be seen. Slab-B was removed from the top of the furnace for investigation and placed on the ground. Substantial deformation of Slab-B illustrates the extent of damage to the slab. The sides of the slabs were covered with RCF, and the visible cracks on the sides of the slabs are the gaps between the RCF blanket pieces.

One of the most informative parts of the fire experiment was the postfire investigation of Slab-B. To discover the failure mode, a thorough investigation was performed by removing concrete to expose the GFRP reinforcing bars. By using a concrete saw, a rectangular prism with dimensions of 120 × 50 × 1,200 mm was cut at both ends of Slab-B.

Regardless of the fully burnt-out resin of the GFRP bars, the failure did not occur due to tensile strength loss. The maximum temperatures at the bottom and top of the reinforcing bars upon failure were 500°C and 350°C, respectively. The experiments on the mechanical properties of GFRP bars at high temperatures showed that GB bars held approximately 85 kN at 400°C (Hajiloo et al. 2018). Given that the estimated existing tensile force in the bars before the fire was 40 kN, the remaining tensile strength was higher than the tensile stress. Moreover, as shown in Fig. 12, the failure was initiated by the pullout of the GFRP bars at the ends of Slab-B. If the bars were to rupture, pullout of the bars could not have occurred. The observed failure was of a similar pattern in all bars with various extents of slip. Fig. 12(a) shows the measured slips at one end of Slab-B, while there was no sign of slip at the far end. The cuts that were made at the end of the slab went through the reinforcing bars as seen in Fig. 12(b). Some bars were completely cut, and others were cut longitudinally in halves. The extent of slip and the situation of the bars convincingly demonstrate that the failure was attributed to the progressive bond loss in the unexposed zone.

The concrete around the reinforcing bars was visually assessed and large splitting cracks were spotted. The cracking condition at the end of Slab-B, in which slip of bars occurred, is shown in Fig. 13(a), and a large crack extended along the half-width of the slab. The cracks all initiated from the reinforcing bars and extended in all directions, although most of the cracks extended

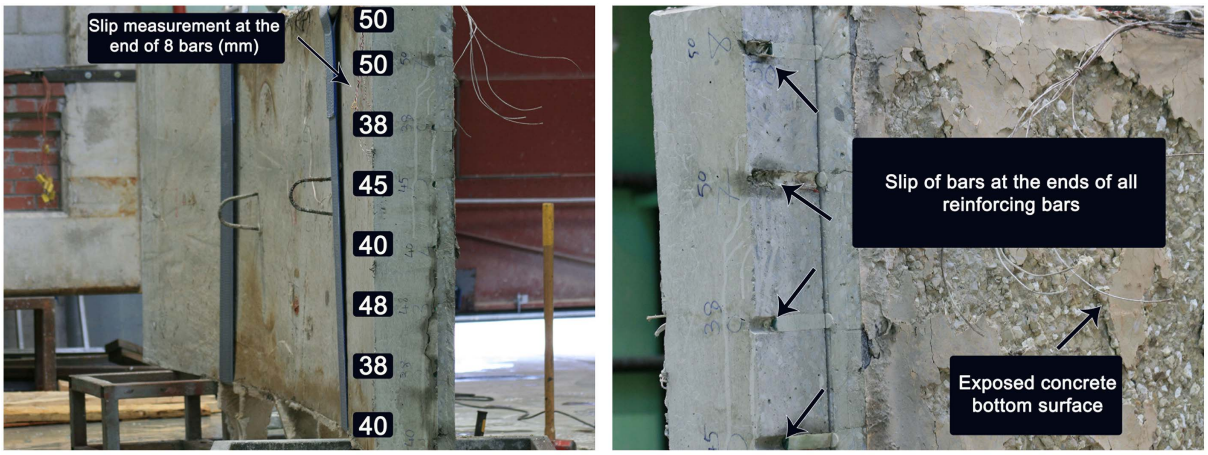

Fig. 12. (a) Slip measurements of bars at one end; and (b) end conditions after test investigations.

J. Compos. Constr., 2019, 23(2): 04019009

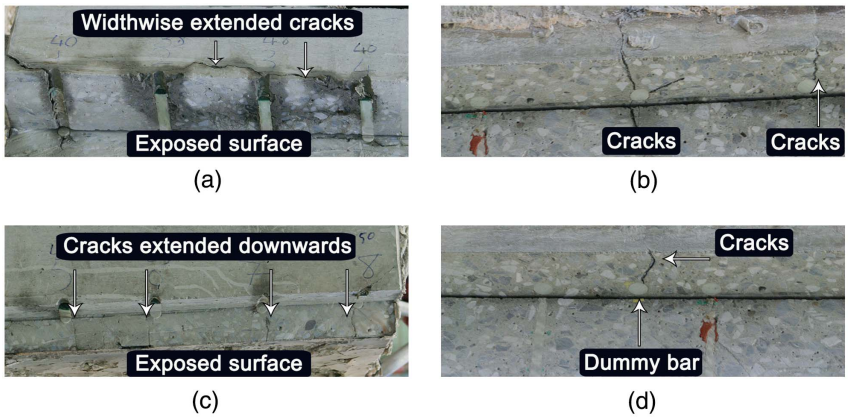

Fig. 13. (a) Widthwise crack; (b) crack initiation around the bars; (c) cracks extended downward; and (d) cracks around the dummy GFRP bar after test investigations of Slab-B.

toward the bottom of the slab. The mentioned crack also extended lengthwise in the plane containing the reinforcing bars. The cracks around the bars shown in Fig. 13(b) at the same end of the slab developed individually extending downward. Fig. 13(c) shows some cracks at the other end of Slab-B where the overall extent and size of the cracks were lower with respect to the other end. This leads to speculations as to whether the slip of the reinforcing bars was the main cause of the substantial cracks. The answer can be found by evaluating the crack shown in Fig. 13(d). The mentioned crack developed around the short dummy GFRP bar that was placed at the end of the slabs to install thermocouples. Since the force in the dummy bar was zero, the cracks developed most likely because of the lateral thermal expansion of the bar. The relation of concrete cover and the extent of thermal-induced lateral cracks in FRP-RC was investigated by Masmoudi et al. (2005) and a ratio of 1.9 was recommended for concrete cover to FRP bar diameter to avoid cracking of concrete at elevated temperatures up to 80°C for the tested materials.

Strains

One of the inherent limits of any experiments at high temperatures is the strain measurement. The mechanism of transferring strains from a reinforcing bar to a strain gauge becomes ineffective as temperature rises (Hajiloo et al. 2017). In fire tests by Nigro et al. (2011b), the strain gauges on top of the main reinforcing bars stopped working after 10 min of fire exposure. The strains increased 1,000 microstrain, from which a considerable portion is believed to be due to free thermal elongation of the reinforcing bars. The precise evaluation of its value is not feasible because of unknown factors such as the coefficient of thermal expansion (CTE) of GFRP bars at high temperatures. It is expected that the different CTEs of a reinforcing bar and concrete cause opposite stresses in the bar and concrete as long as the bond between bar and concrete is effective. Considerable heat-induced tensile stress in the steel reinforcing bars, which was five times as large as the stress from the sustained loads, was shown in the numerical work of Gao et al. (2013). However, the stress level cannot be determined with adequate certainty due to the absolute lack of experimental data. On the other hand, determination of the stress in a reinforcing bar during fire is essential to estimate fire resistance of the RC element. To estimate the total tensile force in the reinforcing bars during the fire, the strains of the bars were thoroughly examined. The discussions and calculations in the following sections were developed based on the results from the two separate sets of full-scale fire tests of GFRP reinforced slabs with 60-mm (Hajiloo et al. 2017) and 40-mm clear concrete cover (current paper).

Heat-Induced Strains

The heat-induced tensile stress in the bars was studied in two steps. First, the readings from the strain gauges were used to estimate the heat-induced stress during the fire until the strain gauges stopped working. Second, the observations during the fire test, deflection behavior, and the strain gauges on the top surface of concrete were used to study the tensile stresses in GFRP after the failure of strain gauges.

Measured Heat-Induced Strains from Strain Gauges. Only the valid strain readings from the fire tests on GFRP-reinforced slabs with 60 and 40 mm were evaluated. The strains in the first 20 min of fire exposure on the slabs with 60-mm cover (Hajiloo et al. 2017) show that the total strain increased from 2,250 to 3,100 microstrains, resulting in an additional 850 microstrains. The thermocouples, which were placed very close to the strain gauges, recorded the temperatures that were used to calculate the free thermal elongation of the bars. At 20 min, temperatures at the bottom and top of the bars were 100°C and 60°C, respectively, resulting in an approximated average of 80°C in the centerline. The ambient temperature of the bars was 20°C at the beginning of fire exposure. The CTE was assumed constant and equal to 7.0×10^{-6} (provided by the manufacturers) to calculate the free thermal elongation at the respective temperatures. Thus, the 60°C temperature increase in the bar centerline created 420-microstrain free thermal elongation. Then, only 430 microstrains of the heat-induced strain can cause additional tensile stress in the GFRP bars, which is resulted from the different CTEs of the concrete and GFRP. The heat-induced tensile stress was approximated to be 27 MPa (5.5 kN) in the first 20 min of the fire. This stress should be compared to the stress (140 MPa) from the sustained loading. This means the heat-induced tensile stress increased by approximately 20% in the first 20 min of fire.

Regarding Slab-B with 40-mm concrete cover, similar calculations show that the tensile stress of the GFRP bars after 15 min of fire exposure increased 22 MPa (4.4 kN). The maximum strain at the end of loading before the fire was 3,100 microstrains, which results in a stress level of 192 MPa equivalent to 39 kN. This means the heat-induced tensile stress increased by approximately 10% in the first 15 min of the fire. Therefore, the results from the calculations on the slabs with 60- and 40-mm cover appear to suggest that the heat-induced tensile stress in the first 20 min of the standard fire was 20% of the existing stress before the fire.

The accuracy of the measured strains (before the fire) was studied by comparing the measured strains with the values from the design calculations. The specified superimposed load was applied in four steps as recommended by CAN/ULC-S101-07 (Underwriters' Laboratories of Canada 2007). Two strain gauges (#3 and #6) were installed at the midspan of Slab-B on two different reinforcing bars. The strains in the GFRP bars that were caused by the sustained loading (before the fire) are shown in Fig. 14(a). The measured strains upon applying the sustained load were very close to the estimated values from the design calculations of the slabs. The cracking moment of the slabs was predicted as 28 kN · m, which can be caused by a superimposed distributed load of 9.8 kN/m and a dead load of 5.8 kN/m. The strains in the bars started to develop when the superimposed load reached 10 kN/m around the cracking load. Fig. 14(b) shows the heat-induced strains in the reinforcing bars with the temperature increase.

Heat-Induced Strains after Strain Gauges Failure. To extend the calculations to the rest of the fire exposure time, wherein the strain gauges had stopped working, two plausible hypotheses are proposed based on the experimental results and the observations. First, the bond between GFRP bar and concrete deteriorates as the temperature at the GFRP-to-concrete interface increases. In the slabs with 60-mm cover, for instance, temperatures reached 200°C and 120°C at the bottom and top of the GFRP bars after 60 min (Hajiloo et al. 2017). If the average temperature in the bar centerline is approximated as 160°C, the retained bond strength is around 20% of the original room temperature bond strength (Hajiloo and Green 2018). Thus, the shear stress transfer mechanism between GFRP bar and concrete is affected, and the differential thermal elongations of the GFRP bar and concrete cause less counteracting influence because the core of the bar can slide alongside the coating. Consequently, an increase in tensile stress of the reinforcing bars during fire exposure can occur only up to the functional temperature of the GFRP-to-concrete interface. Second, the midspan deflection versus the fire exposure time curve presents an important fact in many fire tests (Nigro et al. 2011a; Hajiloo et al. 2017), according to which the deformation of slabs takes place at a higher rate in the early minutes (30 min) of fire than the rest of the fire exposure time. The deformation takes place due to the thermal gradient between the bottom exposed and top unexposed surfaces of the concrete element, which is referred to as bowing effects. At the end of the thermal bowing effects, the deformations of the slabs become relatively stable. The slowly increasing deformations are due to the spread of heat into the concrete and degradation of the material properties such as tensile strength and bond strength of GFRP reinforcing bars. A conclusion based on the previously mentioned hypothesis states that the heat-induced tensile stresses in the reinforcing bars is caused in the early minutes of fire exposure, i.e., 30 min in the experiments by the authors.

Substantial support for the previously discussed hypothesis is found in Fig. 15, where the strains on the top surface of the concrete are presented. Fig. 15(a) shows a consistent strain development at the concrete top surface at the midspan of both slabs where the strains reached 800 microstrains at the end of loading (before fire). The key information can be found in Fig. 15(b), where the strains rapidly increase in only the first 15 min (thermal bowing) and then gradually become steady before the strain gauges stopped working at around 120 min, when the temperature reached on average 60°C on the top surface of concrete.

Strains in the Unexposed Anchor Zones

It was anticipated that the strains of GFRP bars at the unexposed anchor zones would be zero at the start of fire exposure. The strains would increase gradually because of the degradation of the GFRP-to-concrete bond with temperature rise and the free thermal elongations. The approach to measure the strains was effective because the strain gauges endured longer than the strain gauges installed at midspan on the GFRP bars. The heat propagation into the unexposed zones was considerably slower than the fire-exposed areas. Only the useful part of the strains is shown in Fig. 16, where the sensors remained functional and attached to the underlying surface.

To summarize the discussion on the heat-induced strains and the tensile stresses, the tensile stress increase (during fire) in the GFRP reinforcing bars of the slabs with 60 and 40 mm is conservatively estimated to be 50% of the tensile stress caused by the sustained loads. In another conservative approach, the GFRP-to-concrete bond in the fire-exposed areas is considered fully deteriorated. Thus, the entire tensile forces in the GFRP bars transfer to the unexposed anchor zones. This is the basis in the model to determine the fire resistance of the slabs.

New Model to Predict Fire Resistance

The progressive degradation of the GFRP-to-concrete bond in unexposed zones of a fire-exposed GFRP-RC element can be

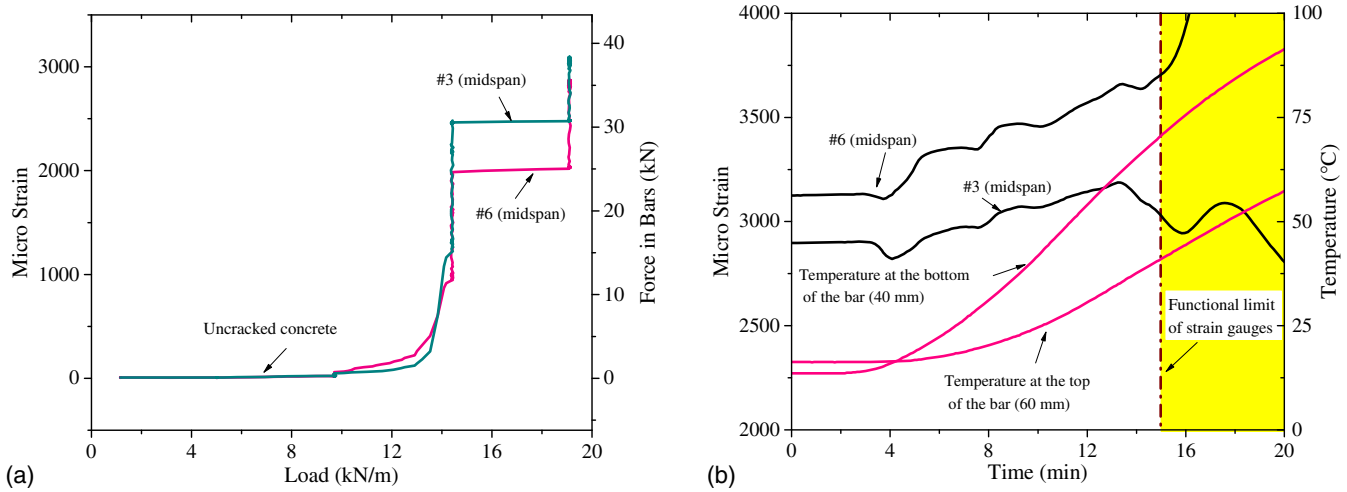

Fig. 14. Strains on the reinforcing bars in the midspan of Slab-B: (a) loading before fire; and (b) during fire.

J. Compos. Constr., 2019, 23(2): 04019009

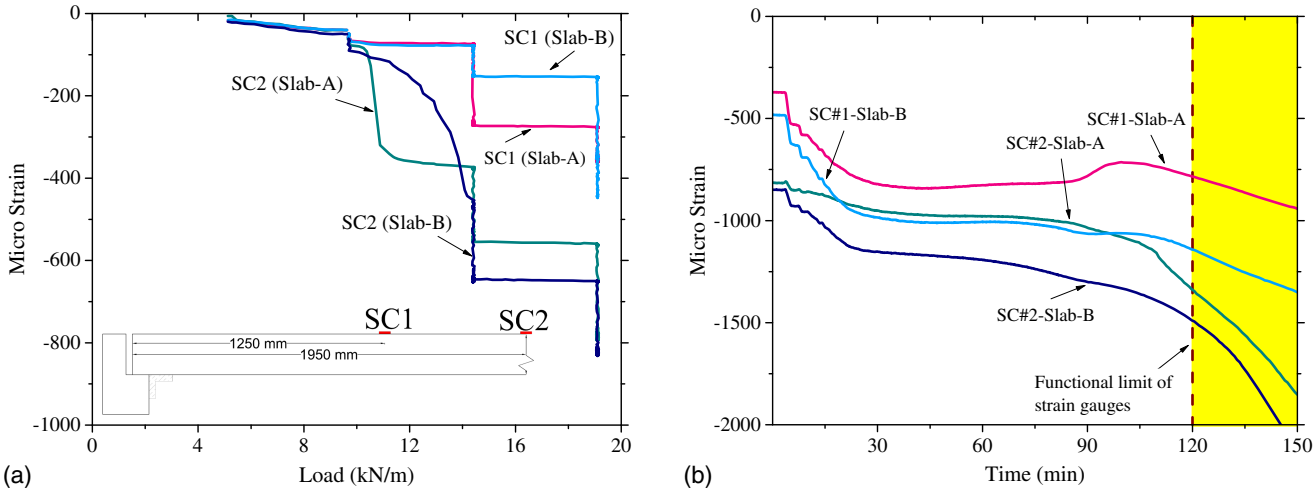

Fig. 15. Strains on the top surface of concrete: (a) loading before fire; and (b) during fire.

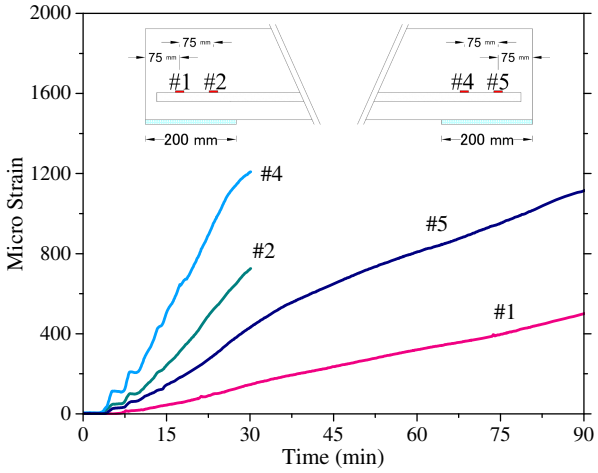

Fig. 16. Strains of the bars at unexposed ends during fire.

estimated if the temperature distribution and bond strength properties at high temperatures are known. The concrete-to-GFRP stress transfer mechanism changes with the increasing temperature. At a certain time after the start of the fire, the tensile force in bars is resisted only by the retained bond strength at the unexposed zones because the GFRP-to-concrete bond has deteriorated in the fire-exposed areas. The ultimate failure of the GFRP-RC is estimated by comparing the retained bond strength against the tensile force in bars. By implementing this method, an analytical model was developed to estimate the fire resistance of GFRP-RC slabs. The full-scale fire tests on GFRP-reinforced slabs with 60-mm clear concrete cover (Hajiloo et al. 2017) and the slabs with 40-mm clear concrete cover provide a sound basis for validating the model.

The prediction of the fire resistance in the present model was achieved in three steps: first, the temperature distribution at any location and any time was determined by numerical heat transfer analysis, which was verified against the experimental results (Hajiloo et al. 2017); second, the retained GFRP-to-concrete bond capacity (pullout) at any time and temperature was determined from the pullout bond tests (Hajiloo and Green 2018); third, the total tensile load in GFRP reinforcing bars was determined to compare with the retained pullout load capacity at any time during fire. The assumptions made in developing the model for GFRP reinforced slabs are as follows:

- The retained tensile strength of the bars at any time is higher than the tensile stress in the bars. Thus, the tensile failure does not occur.
- The bond strength in the fire-exposed areas is entirely deteriorated, and the entire tensile force in the bars is transferred to the unexposed end zones.
- The length of a reinforcing bar in the unexposed zone is divided into several segments at which the temperatures are considered constant.

The bond between GFRP and concrete at elevated temperatures was investigated for three types (GA, GB, and GC) of GFRP reinforcing bars (Hajiloo and Green 2018). The retained bond strength of the bars was fitted using sigmoid curves and they were incorporated into the predictive model. Slab-A and Slab-B were reinforced with GA and GB reinforcing bars. To better demonstrate the procedure that the model adopts, the temperatures and the retained pullout capacity of the GFRP bars at the unexposed zones of the slabs with 60 and 40 mm of cover are shown in Fig. 17. The ends of GFRP bars at the unexposed zones were divided into eight segments, and the temperature in the middle of each segment and the retained pullout capacity of each segment are shown. The drawings of the unexposed length of the bars are provided in Fig. 17 with labeling of the segments and the dimensions. The sum of the retained pullout capacity of the segments was the retained pullout capacity of each bar, which were 57 and 61 kN for the slabs with 60- and 40-mm cover, respectively. The unexposed length of GFRP bars in the slabs with 40 mm of cover was 20 mm longer than the slabs with 60 mm of cover.

The model predictions of the slabs with 60-mm cover (Hajiloo et al. 2017) and the slabs with 40-mm cover are shown in Fig. 18 as a function of the standard fire exposure time. The very comparable bond properties of GA and GB bars are reflected in the model, and the failure time of GA and GB reinforced slabs are quite close. The horizontal lines in Fig. 18 show the measured tensile force in the bars at the beginning and the estimated ultimate force at the end of the fire (150% of the initial force). The failure of the slabs due to the bond loss occurs within the shaded area. Fig. 18(a) shows that the slabs with 60-mm cover are expected to entirely lose the bond strength and fail after 3 h, which correlates well with the experimental results (Hajiloo et al. 2017). Fig. 18(b) shows that the GA

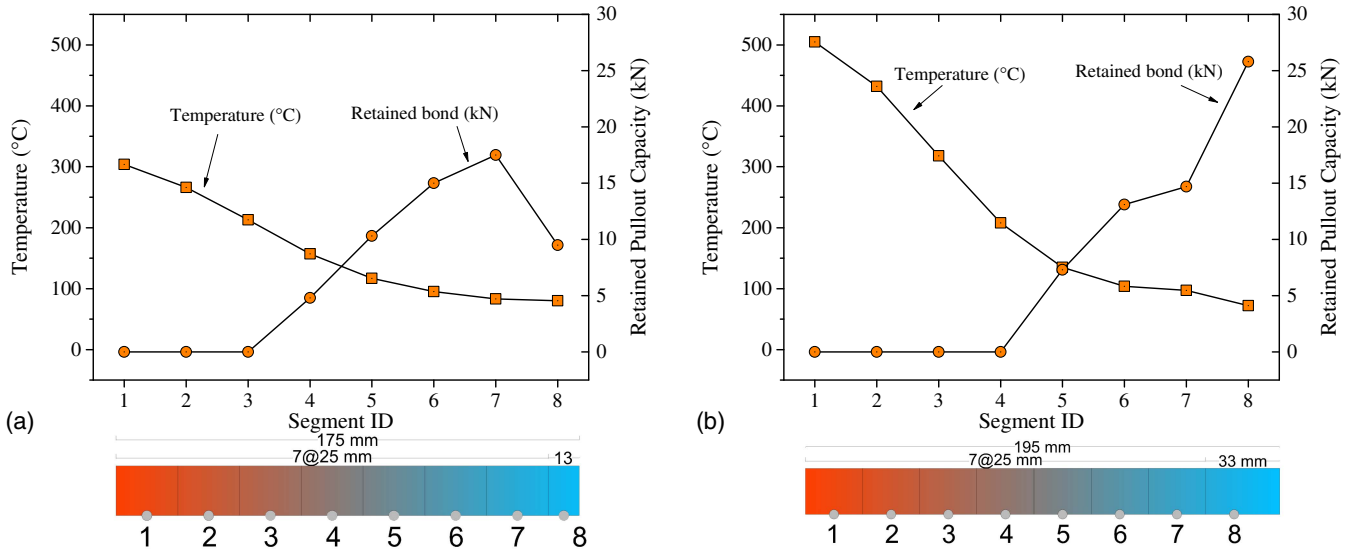

Fig. 17. Temperature and respective retained bond along the unexposed length of GA bars in the slabs with (a) 60 mm of cover; and (b) 40 mm of cover.

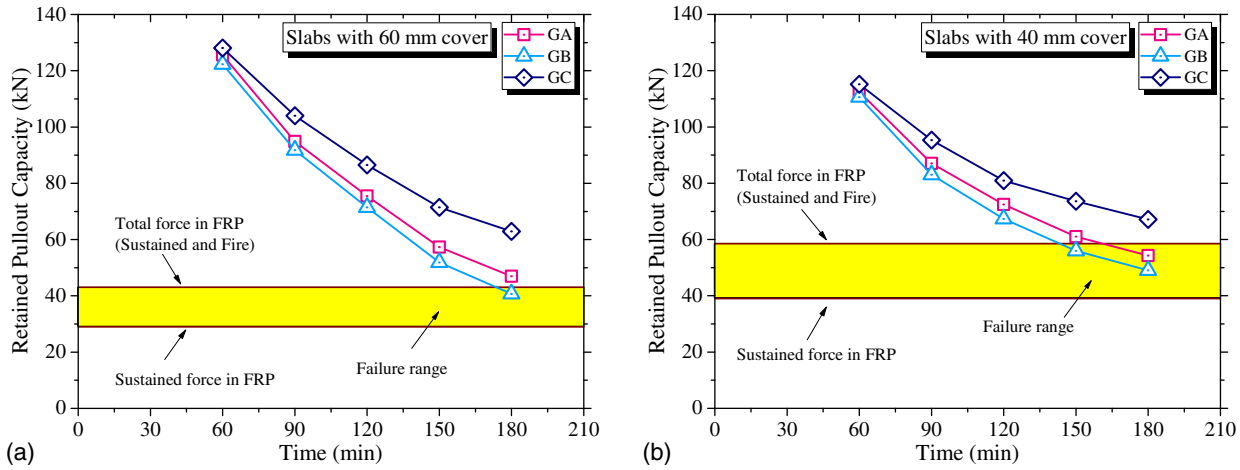

Fig. 18. Estimation of fire resistance of the slabs reinforced with different bar types: (a) 60 mm of cover; and (b) 40 mm of cover.

and GB reinforced slabs with 40-mm cover fail after 2.5 h, which is slightly conservative. Overall, the model predicts the failure time of the tested slabs with a reasonable accuracy margin considering the complexity of the mechanism and the affecting parameters. Because the rigorous determination of tensile forces in the bars during fire has remained unreachable, the approximate approach in this paper based on the measurements and observation from two sets of full-scale standard fire tests appears promising.

Conclusions

To achieve both fire safety and efficient use of GFRP reinforcing bars in construction, two full-scale GFRP-RC slabs with only 40 mm of clear concrete cover were tested under a standard fire. Both slabs obtained 3 h of fire resistance while subjected to sustained loading that was greater than the expected service load based on serviceability design criteria (deflection and crack control). The slabs were provided with only 200-mm-long unexposed (cool) anchor zones at the ends of the slabs.

- The loaded slabs endured 3 h of ASTM E119 standard fire exposure. One of the slabs failed due to bond failure.
- The concrete and the ends of the bars were effectively protected to provide adequate anchorage during the fire test. The temperature of GFRP bars in the exposed zone (600°C) substantially reduced when compared with the temperature at 100-mm distance into the unexposed zone (200°C).
- The temperature measurements in the unexposed zone showed that GFRP bars can be safely used as negative reinforcing bars in multispan slabs or beams.
- The retained bond strength and the temperature gradients in the unexposed zones emphasize the effects of unexposed zones. By providing a proper unexposed anchorage length at the ends of a GFRP-reinforced slab, the concrete cover can be reduced. The practical recommendation is to make GFRP bars continuous over walls or columns within a fire compartment.
- The increase in the tensile force of GFRP bars during fire is conservatively estimated as 50% of the sustained load. The estimated total tensile force in the bars is necessary to estimate the fire resistance of GFRP reinforced slabs.

J. Compos. Constr., 2019, 23(2): 04019009

- The model conservatively estimates the failure time of the slabs when the GFRP bars lose their bond to the concrete in the unexposed anchor zone.

Overall, this study provides information regarding the fire performance of GFRP-RC slabs and shows that comparable fire resistance to steel-reinforced concrete can be obtained if an engineered design is implemented by providing practical unexposed zones and avoiding splicing of bars within the exposed zones.

Acknowledgments

The authors would like to thank the Natural Sciences and Engineering Research Council of Canada (NSERC), Pultrall Inc., and BP Composites for financial and material support. The authors also appreciate the insightful advice of Dr. Benmokrane and the cooperation of Dr. Mohammad from Sherbrooke University. The authors thank the technical staff of the Fire Research Laboratory at NRC. The contribution of Dr. Gales is appreciated.

References

Abbasi, A., and P. J. Hogg. 2006. "Fire testing of concrete beams with fibre reinforced plastic rebar." *Composites Part A* 37 (8): 1142–1150. https://doi.org/10.1016/j.compositesa.2005.05.029.

ACI (American Concrete Institute). 2015. *Guide for the design and construction of concrete reinforced with FRP bars.* ACI 440.1R. Farmington Hills, MI: ACI.

ASTM. 2015. *Standard test methods for fire tests of building construction and materials.* ASTM E119. West Conshohocken, PA: ASTM.

Bisby, L. A., and V. K. Kodur. 2007. "Evaluating the fire endurance of concrete slabs reinforced with FRP bars: Considerations for a holistic approach." *Composites Part B* 38 (5): 547–558. https://doi.org/10.1016/j.compositesb.2006.07.013.

CSA (Canadian Standards Association). 2010. *Specification for fibre-reinforced polymers.* CSA S807. Mississauga, ON, Canada: CSA.

CSA (Canadian Standards Association). 2012. *Design and construction of building components with fibre-reinforced polymers.* CSA S806. Mississauga, ON, Canada: CSA.

CSA (Canadian Standards Association). 2015. *Concrete materials and methods of concrete construction/test methods and standard practices for concrete*. CSA A23.1-14/A23.2-14. Mississauga, ON, Canada: CSA.

Gao, W., J.-G. Dai, J. Teng, and G. Chen. 2013. "Finite element modeling of reinforced concrete beams exposed to fire." *Eng. Struct.* 52: 488–501. https://doi.org/10.1016/j.engstruct.2013.03.017.

Hajiloo, H., and M. Green. 2018. "Bond strength of GFRP reinforcing bars at high temperatures with implications for performance in fire." *J. Compos. Constr.* 22 (6): 04018055. https://doi.org/10.1061/(ASCE)CC.1943-5614.0000897.

Hajiloo, H., M. F. Green, and J. Gales. 2018. "Mechanical properties of GFRP reinforcing bars at high temperatures." *Constr. Build. Mater.* 162: 142–154. https://doi.org/10.1016/j.conbuildmat.2017.12.025.

Hajiloo, H., M. F. Green, M. Noël, N. Bénichou, and M. Sultan. 2017. "Fire tests on full-scale FRP reinforced concrete slabs." *Compos. Struct.* 179: 705–719. https://doi.org/10.1016/j.compstruct.2017.07.060.

ISIS (Intelligent Sensing for Innovative Structures) Canada. 2007. *Reinforcing concrete structures with fibre reinforced polymers. Design Manual 3*. Winnipeg, MB, Canada: ISIS Canada.

Kumahara, S., Y. Masuda, H. Tanano, and A. Shimizu. 1993. "Tensile strength of continuous fiber bar under high temperature." *ACI Spec. Publ.* 138: 731–742.

Masmoudi, R., A. Zaidi, and P. Gérard. 2005. "Transverse thermal expansion of FRP bars embedded in concrete." *J. Compos. Constr.* 9 (5): 377–387. https://doi.org/10.1061/(ASCE)1090-0268(2005)9:5(377).

Nigro, E., G. Cefarelli, A. Bilotta, G. Manfredi, and E. Cosenza. 2011a. "Fire resistance of concrete slabs reinforced with FRP bars. Part I: Experimental investigations on the mechanical behavior." *Composites Part B* 42 (6): 1739–1750. https://doi.org/10.1016/j.compositesb.2011.02.025.

Nigro, E., G. Cefarelli, A. Bilotta, G. Manfredi, and E. Cosenza. 2011b. "Fire resistance of concrete slabs reinforced with FRP bars. Part II: Experimental results and numerical simulations on the thermal field." *Composites Part B* 42 (6): 1751–1763. https://doi.org/10.1016/j.compositesb.2011.02.026.

Underwriters' Laboratories of Canada. 2007. *Standard methods of fire endurance tests of building construction and materials*. CAN/ULC-S101-07. Toronto, ON, Canada: Underwriters' Laboratories of Canada.

Weber, A. 2008. "Fire-resistance tests on composite rebars." In *Proc., Int. Conf. on FRP Composites in Civil Engineering (CICE2008)*. Zurich, Switzerland: EMPA.